JOURNAL OF MATERIALS SCIENCE 28 (1993) 4595–4606

Debonding microprocesses and interfacial strength in particle-filled polymer materials

A. V. ZHUK, N. N. KNUNYANTS, V. G. OSHMYAN, V. A. TOPOLKARAEV, A. A. BERLIN
Institute of Chemical Physics, Russian Academy of Sciences, 4 Kosygin Str., Moscow, 117977, Russia

Griffith energy theory was developed for analysis of crack propagation along an interface in polymers filled with rigid spherical inclusions. A polydisperse structural model was used for stress–strain distribution analysis of composite materials. Experiments were performed on glass-bead filled polyethylene and polypropylene and epoxy resin. The dependence of debonding stresses and angles on contraction stress, friction, particle diameter and material characteristics were analysed.

1. Introduction

Strength and plastic behaviour of particle-filled polymeric materials are subjected to a considerable extent to microprocesses of deformation and fracture taking place in the close vicinity to inclusions [1–5]. One of the main aspects of these processes is a debonding of a polymer matrix from inclusions which leads to alteration of the local stress–strain distribution (SSD) [4, 6–8] and predetermines the subsequent fracture process. The formation of interfacial debonding in different filled polymer systems may not only be an undesirable fracture source but also an effective canal for energy dissipation [9].

Based upon existent data it is possible to distinguish the two main characteristics of the debonding process: a debonding stress and a part of the debonding interface. The few investigations reported in this field point to the necessity for more detailed analysis of the debonding mechanism and its dependence on the material physical parameters, the state of the interface, inclusion size and content, and effect of external conditions.

The fracture mechanism analysis requires proper choice of criteria to be made. The known criteria of boundary fracture can be divided into two main groups: stress criteria based on the calculation of the local stress intensities, and energy criteria based upon the Griffith theory [10].

The present work was devoted to the development of the energy Griffith theory and experimental analysis of crack propagation along the interface in polymers filled with rigid spherical inclusions. The following factors which have an influence on the relative part of the debonding interface (debonding angle, ψ_d) and debonding stress, σ_d, were studied: size and volume fraction of the filler, interfacial surface energy, thermal contraction stress, and the presence of friction between the sides of the propagating interfacial fracture.

Special attention should be paid to various restrictions imposed to simplify and clarify the undertaken analysis: (1) the theoretical analysis of the debonding process is developed in the elastic case within the framework of a Hashin polydisperse model; (2) the defect nucleation mechanism, and the size and distribution of defects are not discussed; (3) the possibility of the alteration of surface energy during debonding propagation, which can be caused by microplastic flow near the debonding tip, by variation of the crack propagation rate and by the geometry of an inclusion, is not taken into consideration.

2. Theoretical analysis

2.1. Theoretical model description and boundary conditions

The polydisperse structural model suggested by Hashin [11] was used for strain–stress distribution analysis of composite materials. It is assumed that all the volume can be divided into similar domains, that may have only boundary contact points (Fig. 1a). For particle-filled composites it is natural to consider a spherical inclusion within a cell structure forming a spherical shell. The ratio of particle radius, R, to the shell radius, A, (Fig. 1b) is related to volume filler content, α

$$(R/A)^3 = \alpha \quad (1)$$

Let us state the problem concerning the description of continuous displacement fields $\boldsymbol{u}(x)$ in heterogeneous materials of polydisperse structure. Such fields provide identical SSD in different cells. It is not difficult to prove that the following correlation is necessary and sufficient for such fields

$$\boldsymbol{u}(x)|_{x\in S} = \boldsymbol{u}_0 + \boldsymbol{u}_1 x_1 + \boldsymbol{u}_2 x_2 + \boldsymbol{u}_3 x_3 \quad (2)$$

Indeed, Equation 2 allows us to construct the displacement field with identical SSD in different cells.

0022–2461

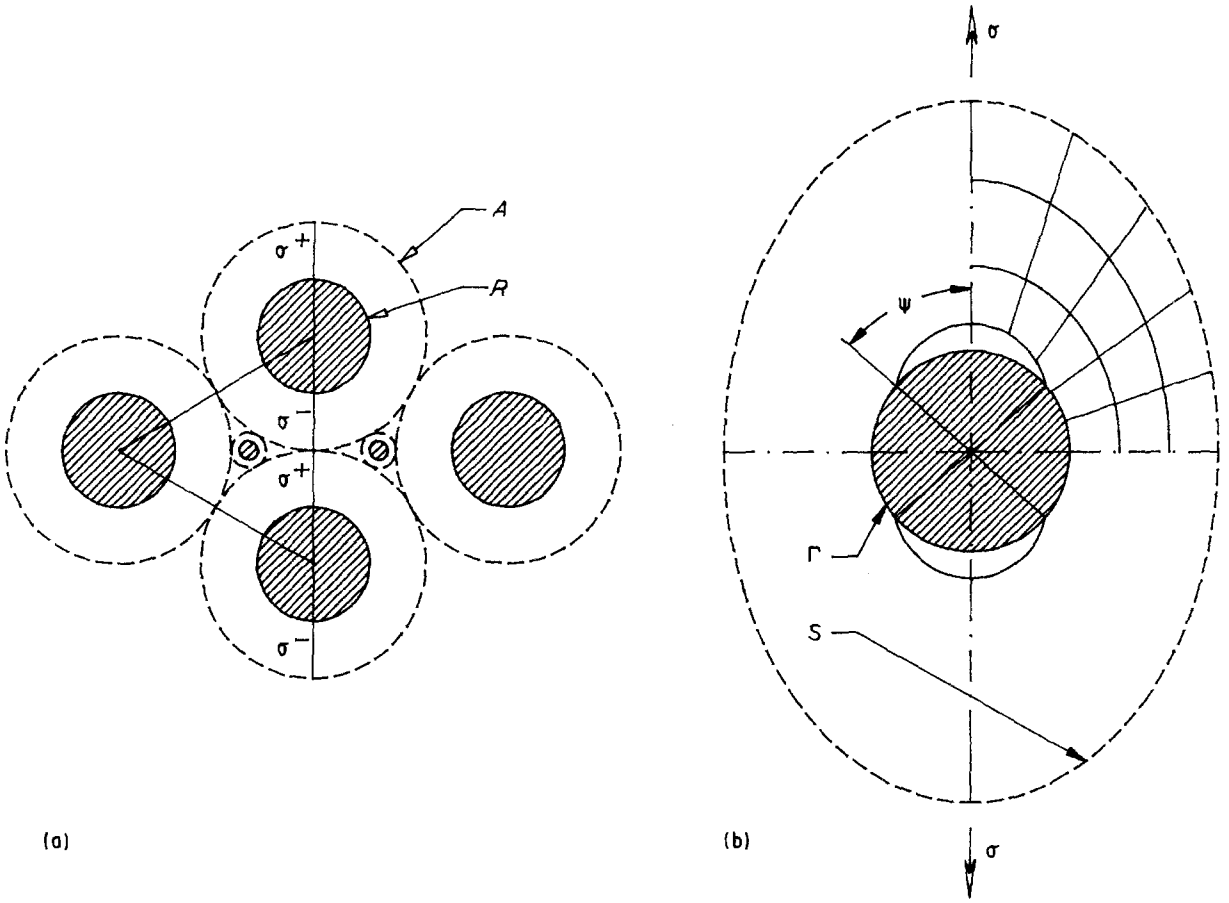

Figure 1 Schematic representation of spherical shell configuration given by Hashin [11]: (a) polydispersed model and (b) deformed elementary shell with debonding angle ψ.

Inversely, if a continuous displacement field $\boldsymbol{u}$ gives equal strain fields in different cells, it is easy to see the necessity of Equation 2 by taking into account all triangles of adjacent shells.

Furthermore, central symmetry of the cell leads to central symmetry of stress fields (Fig. 1a) and, consequently, to their equality in the adjacent points: $\sigma^+ = \sigma^-$. The above considerations are convincing arguments for the SSD description in the polydisperse composite structure by the displacement fields of the class under review.

In comparison with regular structure composites, when deformation is described by solving the continuum media mechanics boundary problem for a repeated element with periodic boundary conditions, for the polydisperse structure composite, such an element is a spherical shell and the boundary conditions of Equation 2, apply.

In the present study the cylindrical symmetrical boundary problem is solved using the finite elements method for the equilibrium equations

$$\frac{\partial \sigma_{ij}}{\partial x_j} = 0 \tag{3}$$

with the following conditions at the cell boundary

$$u_1|_S = \varepsilon x_1, \quad u_2|_S = -\delta x_2,$$
$$u_3|_S = -\delta x_3 \tag{4}$$

The particles are supposed to be rigid and debonded from the matrix inside a certain symmetric volume angle (Fig. 1b). Friction between debonded parts of the surface is assumed to be neglected. So, the boundary conditions at the inside surface, Γ, of the spherical shell can be given as follows.

When $\theta \geq \psi$

$$\boldsymbol{u}|_\Gamma = 0 \tag{5a}$$

when $\theta < \psi$

$$\sigma_{r\theta}|_\Gamma = 0 \tag{5b}$$

$$\sigma_{rr}|_\Gamma = 0 \quad \text{if } u_r \geq 0 \tag{5c}$$

or

$$u_r|_\Gamma = 0 \quad \text{otherwise.} \tag{5d}$$

In accordance with cylindrical symmetry $u_\varphi = \sigma_{r\phi} = \sigma_{\theta\varphi} = 0$. The central symmetry allows us to place the restriction that the angles do not exceed $\pi/2$. The domain $R \leq r \leq A$, $0 \leq \theta \leq \pi/2$ is divided into the rectangular $r_j \leq r \leq r_{j+1}$, $\theta_i \leq \theta \leq \theta_{i+1}$, in which the displacement components u_r, u_θ are approximated by the following functions

$$u_r = r(A_r r + B_r\theta + C_r r\theta + D_r) \tag{6a}$$

$$u_\theta = (A_\theta r + B_\theta\theta + C_\theta r\theta + D_\theta) r \sin\theta \tag{6b}$$

The values u_r, u_θ at the knots of the network and the corresponding coefficients in Equations 6a and b are obtained from the condition of elastic energy minimum

$$W = 4\pi \int_R^A dr \int_0^{\pi/2} d\theta r^2 \sin\theta \sigma_{ij}\varepsilon_{ij}/2 \tag{7}$$

The value of longitudinal, ε, and transverse, δ, macrodeformations are determined by the uniaxial tension conditions

$$\langle\sigma_{11}\rangle = 1, \quad \langle\sigma_{22}\rangle = \langle\sigma_{33}\rangle = 0 \quad (8)$$

(angle brackets denote the volume average).

2.2. The energy criterion of interface crack growth

Let γ be the debonding energy density. Free energy decrease

$$F(R, \sigma, E, \psi, \alpha, \nu, \Delta\alpha\Delta T) = F_S - F_e \quad (9)$$

is regarded as a crack growth condition: ψ is the debonding angle, R the inclusion radius, σ the external tensile stress, E, ν the matrix Young's modulus and Poisson's ratio, $\Delta\alpha$ the difference between matrix (α_m) and inclusion ($\alpha_i \ll \alpha_m$) thermal extension coefficients, ΔT the difference between manufacturing and use temperatures, F_S the surface energy necessary for the formation of two debondings inside the angle ψ or cone (Fig. 1b) with a solid angle $S = 4\pi(1 - \cos\psi)$

$$F_S = 4\pi(1 - \cos\psi)R^2\gamma = S(\psi)R^2\gamma \quad (10)$$

F_e is the elastic energy of spherical shell

$$F_e = R^3 W_c(\sigma, E, \psi, \alpha, \nu, \Delta\alpha\Delta T) \quad (11)$$

In the absence of thermal contraction: $\Delta\alpha\Delta T = 0$, F_e is proportional to σ^2/E

$$F_e = \frac{\sigma^2}{E} R^3 W(\psi, \alpha, \nu) \quad (12)$$

W_C and W are the shell deformation energies calculated for $R = 1$ (Equation 11) and $R = 1$, $\sigma = 1$, $E = 1$ (Equation 12).

Furthermore, the clearer formula (Equation 12) will be used if there are no special notations. In this case, free energy may be expressed as

$$F = \frac{\sigma^2}{E} R^3[\bar{\gamma}S(\psi) - W(\psi, \alpha, \nu)] \quad (13)$$

where

$$\bar{\gamma} = \frac{E\gamma}{\sigma^2 R} \quad (14)$$

is the reduced surface energy; $\bar{\gamma}$ determines the energy conditions of debonding growth.

In every concrete calculation, Poisson's ratio was assumed to be 0.33. For this reason, ν will not be further used. In the main the analysis was carried out for weakly interacted inclusions ($\alpha = 3.5\%$). Fig. 2 shows the dependence of angle, ψ, on $dW(\psi)/d\psi$ and $\bar{\gamma}\,dS(\psi)/d\psi$ at different $\bar{\gamma}$. The curves do not intersect each other if $\bar{\gamma} \geq \bar{\gamma}_{cr} \simeq 1.23$. Thus the free energy monotonically increases and, therefore, the presence of any defects does not lead to adhesive failure. If $\bar{\gamma} < \bar{\gamma}_{cr}$, the curves intersect at two points. The first one, ψ_1, corresponds to the maximum of free energy (Fig. 3) and is equal to the minimum angle value of the initial defect capable of initiating adhesive failure. At point ψ_2, free energy reaches a minimum and, therefore, further development of the debonding crack becomes disadvantageous. Variation of ψ_1 and ψ_2 with $\bar{\gamma}$ is represented in Fig. 4 (curve 1). It can be seen that $\psi_1 \to 0°$ and $\psi_2 \to 90°$ when $\bar{\gamma} \to 0$, i.e. particle radius and load increase or γ decrease leads to energy advantageous to small defect propagation up to high end angles.

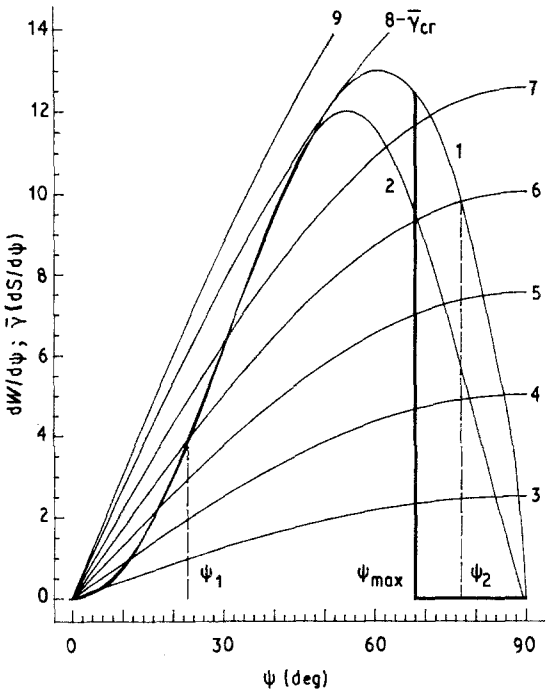

Figure 2 Dependence of angle, ψ, on elastic energy $dW(\psi)/d\psi$. (1) Finite element method calculations; (2) Gent approximation: $W = 8\sin^3(\psi)$ [12], and the whole reduced surface energy $\bar{\gamma}[dS(\psi)/d\psi]$ ($\bar{\gamma}$ = (3) 0.2, (4) 0.4, (5) 0.6, (6) 0.8 (7) 1.0, (8) 1.23, (9) 1.4. The vertical line ($\psi_{max} = 68°$) indicates the interruption of Curve 1 by friction.

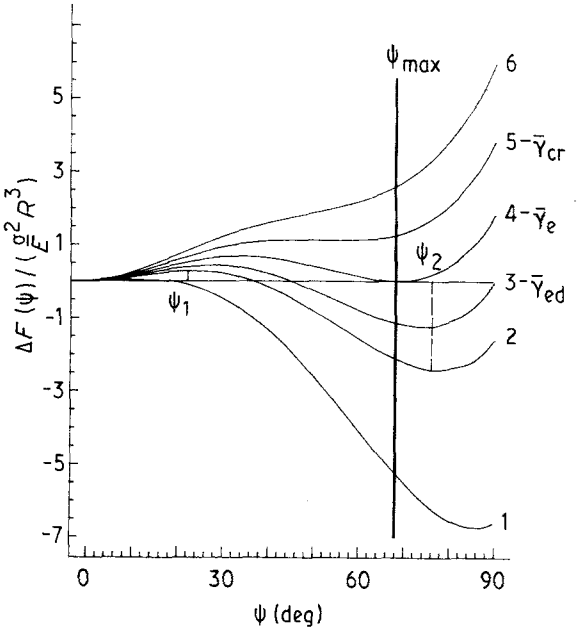

Figure 3 Free-energy dependence, ΔF ($\bar{\gamma}$ = (1) 0.4, (2) 0.8, (3) 0.93, (4) 1.07, (5) 1.23, (6) 1.4) upon debonding angle ψ (ψ_1 = maximum, ψ_2 = minimum).

An approximate analytical description of the connection between the elastic energy and the debonding

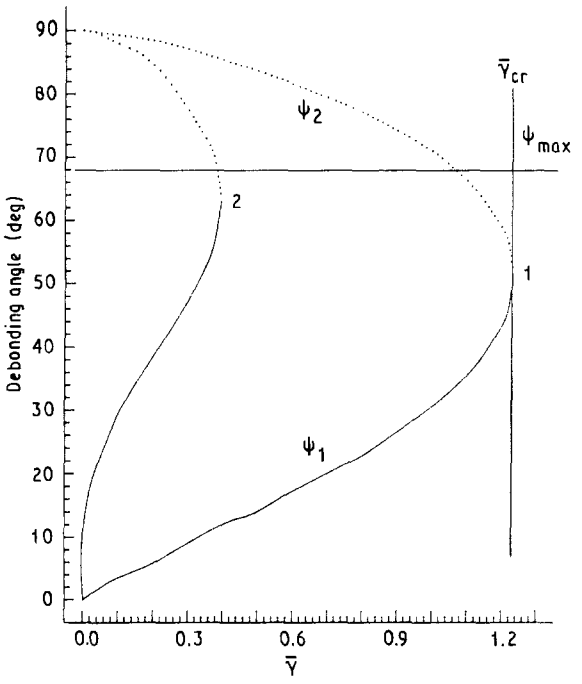

Figure 4 (——) Initial, ψ_1, and (. . .) final, ψ_2, debonding angle dependence upon reduced surface energy, $\bar{\gamma}$: (1) in the absence of thermal contraction; (2) for debonding stresses $\sigma_d < \sigma_c/q_0$. $\bar{\gamma}_{cr}$ defines the range of $\bar{\gamma}$ values ($0 < \bar{\gamma} < \bar{\gamma}_{cr}$) energetically advantageous for debonding.

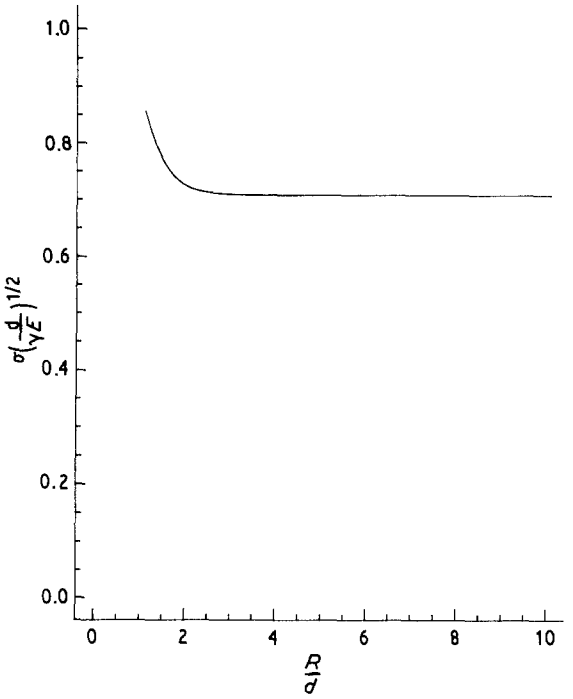

Figure 5 Dependence of theoretical debonding stress, σ_d, on inclusion radius, R, calculated assuming a fixed defect size (d = const.).

angle (DA) was proposed by Gent [12]

$$\Delta W = W(\psi) - W(0) = kq_0^2 \sin^3(\psi), \quad (kq_0^2 \simeq 8) \tag{15}$$

by estimation of the "unloaded" volume value (Fig. 2). It is seen that Equation 15 is a rather good approximation for $dW(\psi)$. However, it does not allow analysis of the conditions of debonding propagation with increasing filler content, the existence of thermal contraction stress and friction between the faces of appearing debonding crack.

2.3. The scale factor

If the defect radius, $d(\psi_0 = d/R)$, is assumed to be independent from the inclusion radius, R, one can calculate the adhesive strength, σ_d, as a function of R (Fig. 5). A marked dependence is observed only at $d \sim R$. In the common case

$$1/(\bar{\gamma}) = \frac{\sigma^2 R}{E\gamma} = \left(\frac{dS(\psi)}{d\psi}\right)\Big/\left(\frac{dW(\psi)}{d\psi}\right) = \frac{dS(\psi)}{dW(\psi)} \tag{16}$$

that leads to

$$\frac{\sigma^2 d}{E\gamma} = \frac{dS}{dW}\frac{d}{R} = \frac{dS}{dW}\psi_0 \tag{17}$$

When $\psi_0 \to 0$ the problem of the matrix debonding from the spherical inclusion converts to the problem of debonding from the rigid plane. According to its solution [12]

$$\sigma^2 = \frac{4\pi\gamma E}{3dkq_0^2} \tag{18}$$

where k is a value slightly dependent on Poisson's ratio ($k = 2$ at $\nu = 0.5$, $k = 2.29$ at $\nu = 0.33$), q_0 is the coefficient of the local overstress (on the pole of the single spherical inclusion $q_0 \simeq 2$), which in the normal case can be evaluated from the SSD analysis in the composite material and depends on geometry, filler content and aggregation. Solution of the debonding problem for two elastic media divided by a plane was obtained by Mossakovsky and Rybka [13]. So, at $d/R \ll 1$, the dependence of σ_d on filler radius disappears.

The defect size may depend on filler radius and, in particular, be proportional to it ($\psi_0 = d/R$ = const.). This assumption leads to the linear dependence of the debonding stress (DS), σ_d, on $1/R^{1/2}$. Such a dependence was observed experimentally for filled elastomers [12].

Davidge and Green [14] used integral criteria of energy balance for the scale factor evaluation. According to this, debonding occurs up the angle ψ_e, if the released elastic energy is sufficient for the formation of a new surface

$$\Delta F = \Delta F_S - \Delta F_e = 4\pi(1 - \cos\psi)R^2\gamma - F_e(0) + F_e(\psi) \leq 0 \tag{19}$$

The value of reduced surface energy, $\bar{\gamma}_e$, when Equation 19 is valid for the first time, is 1.07, and the corresponding DA, $\psi_e = 68.5°$ (Fig. 3). The integral criteria of energetic balance also lead to the inverse square root scale dependence of $\sigma_d(E\gamma/\sigma^2 R = \bar{\gamma}_e =$ const.). One of the peculiarities of this approach is that complete debonding takes place if $\bar{\gamma} \leq \bar{\gamma}_{ed} = 0.93$ (the existence of such a critical value is improbable).

2.4. The effect of filler volume content

$W(\psi)/d\psi$ dependencies at different filler contents, α, are presented in Fig. 6. One can see the permanent

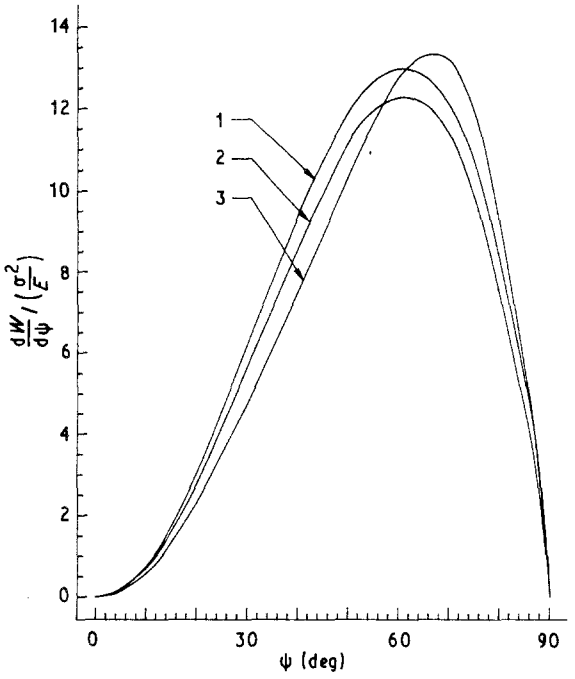

Figure 6 Dependence of spherical shell elastic energy, $dW(\psi)/d\psi$, on debonding angle, ψ, at different filler contents: (1) 3.5 vol %; (2) 10 vol %; (3) 20 vol %.

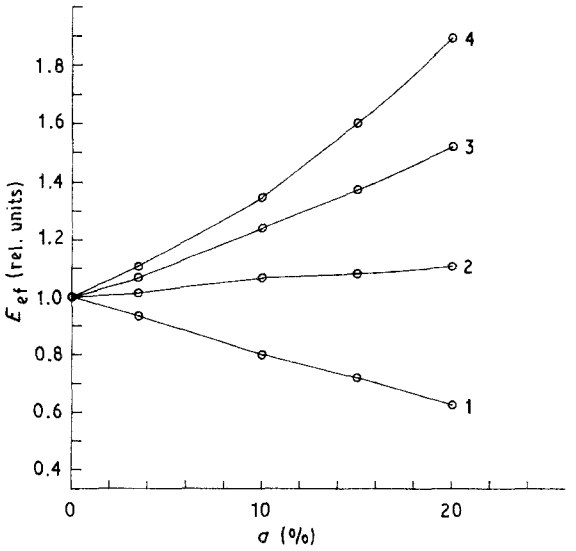

Figure 7 The relative Young's modulus, E_{ef}, dependence upon rigid filler content, a, for different debonding angles ψ_d = (1) 90° (complete debonded), (2) 54°, (3) 36°, (4) 0° (ideal adhesion).

character of these dependencies with filler content growth (at least up to 20 vol %). The proper analysis shows a slight increase of DS for fixed initial crack size with filling. Low sensitivity of initial, ψ_1, and final, ψ_2, debonding angles to the filler content is caused by averaging of the influence of neighbouring inclusions on the SSD. Probably this effect is a consequence of spherical shell size distribution in a polydisperse model. SSD in a composite of periodical structure is more sensitive to filler content. Local overstress coefficient dependences on filler concentration for the periodic model with cubic inclusions were calculated and are presented elsewhere [15].

2.5. The effect of filler volume content and DA on the elastic modulus

The solution of Equations 3–5 allows calculation of an effective composite stiffness, E_{ef} (Fig. 7) at any filling and degree of adhesive connection (debonding angle, ψ_d). It should be noted that E_{ef} varies considerably with DA and may increase or decrease depending on its value. The given curves are analogous to the dependences obtained using other models [16–18]. It is important to mention that increasing DA leads to a considerable drop in effective composite stiffness.

2.6. The influence of friction between crack faces upon DA

The above analysis did not take into account the friction between the debonding faces: free tangential displacements were allowed even when they were forced together (boundary conditions in Equation 5). In the filled composites, such behaviour may be realized only as a result of special treatment of the particle surface. In the opposite case, friction cannot be neglected.

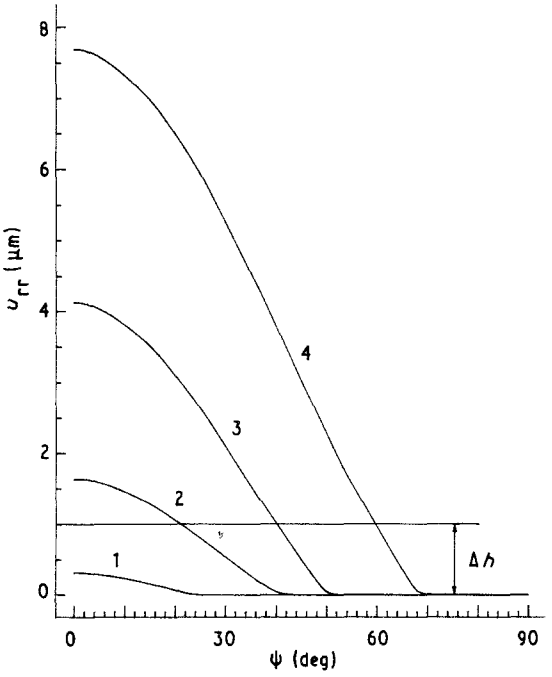

Figure 8 Calculated radial displacement, u_r, of a polymer matrix from a spherical filler surface (D = 52 μm) as a function of angle, ψ, in the presence of contraction stress under different loads, σ = (1) 7 kg mm^{-2}, (2) 10 kg mm^{-2}, (3) 15 kg mm^{-2}, (4) without contraction stress under load 15 kg mm^{-2}. (——) The mean height of the surface relief for the polydimethyl-dichlorosilane covering ($dh \simeq 1$ μm).

Displacement field analysis shows (Fig. 8) that debonding leads to matrix detachment from the particle surface up to the angle $\psi_{max} = 68°$. Hence friction cannot change the energy conditions of crack propagation in this angle region. However, the following exfoliation does not lead to further detachment, only to surface shifts. So SSD and elastic energy change is terminated if the friction coefficient is sufficiently high (Fig. 2) and further debonding becomes energetically disadvantageous. At low friction, the DAs may change up to 90°. In the present case (high friction), angles are

close to $\psi_{max} = 68°$ (maximum DA) for all $\bar{\gamma} < \bar{\gamma}_{cr}$. Thus ψ_d will be independent of inclusion radius, DS and polymer matrix properties.

2.7. Thermal contraction effect

The effect of thermal contraction stress, σ_c

$$\sigma_c = \sigma_{rr}^{r=R} = \frac{2E}{(1+\nu)} \Delta\alpha\Delta T \left(\frac{R}{r}\right)^3 \Big|_{r=R} \quad (20)$$

(r is the distance from a particle centre and R its radius), on the energy balance of interface crack propagation was analysed. Contraction strains, ε_c, for the matrix ($\varepsilon_{cm} = \alpha_m \Delta T$) and filler ($\varepsilon_{cf} = \alpha_f \Delta T$) in the unloaded state are equal to 1% and 0%, respectively ($\sigma_c = 4.5\,kg\,mm^{-2}$ when $E = 300\,kg\,mm^{-2}$). The dependence of $dF_e/d\psi$ on angle ψ for different loads is represented in Fig. 9. It is clear that the dependence of F_e on σ and E becomes more complete in the presence of contraction.

If DS considerably exceeds the contraction stress ($\sigma_d > 4-5\sigma_c$) a contribution of contraction into elastic energy becomes insignificant and the $[dF_e(\psi)/d\psi]/[(\sigma^2/E)R^3]$ curves become close to the $dW(\psi)/d\psi$ curve (Fig. 9). Therefore, contraction may be neglected for high loads.

If external and contraction stresses are of the same order, the latter must be taken into account in calculations. Displacement field analysis (Fig. 8) shows that at low friction, exfoliation may occur without detachment, due to release of shear deformation energy. The stress threshold $\sigma_d \leq \sigma_c/q_0$, restricted by the top external load, ensures that debonding only occurred by a shear mechanism. The dependence of ψ_1 and ψ_2 on $\bar{\gamma}$ for low adhesive strength ($\sigma_d \leq \sigma_c/q_0$) is represented in Fig. 4 (Curve 2). Significant diminution of $\bar{\gamma}_{cr}$ is observed. A comparison of energy conditions of debonding for a given defect size $\psi_1 = 10°$ in the presence of contraction ($\varepsilon_c^{r\to\infty} = 1\%$), and without it shows that contraction raises the stress of crack propagation by 3.7-fold. Some shift of elastic energy release maximum into large angles for low DSs, lead to an increase of final DAs, ψ_2, for the same initial ones, ψ_1.

2.8. Joint thermal contraction and friction effect

If we take into consideration friction between the faces of a growing crack in the presence of contraction, the maximum DA, $\psi_{max}(\sigma)$, is a growing function of applied stress, σ. The maximum debonding angle tends to $\psi_{max} = \lim \psi_{max}(\sigma)$, corresponding to an absence of contraction (Figs 8 and 10).

The existence of these two factors restricts the minimum DS, because in the presence of higher friction it cannot be less than σ_c/q_0. The last condition corresponds to the onset of debonding of the matrix from the inclusion pole.

Thus, due to the presence of contraction and friction the crack behaviour on the spherical interface can be described in following way: from a certain stress level, an initial defect grows up to an angle of $\psi_d = \psi_{max}(\sigma)$ for a short time; further increase of DA is stipulated by the growing applied load, and ψ_d tends to ψ_{max}.

2.9. The effect of polymer coating thickness

An analysis of the influence of soft interface layers on the SSD in the neighbourhood of an inclusion was

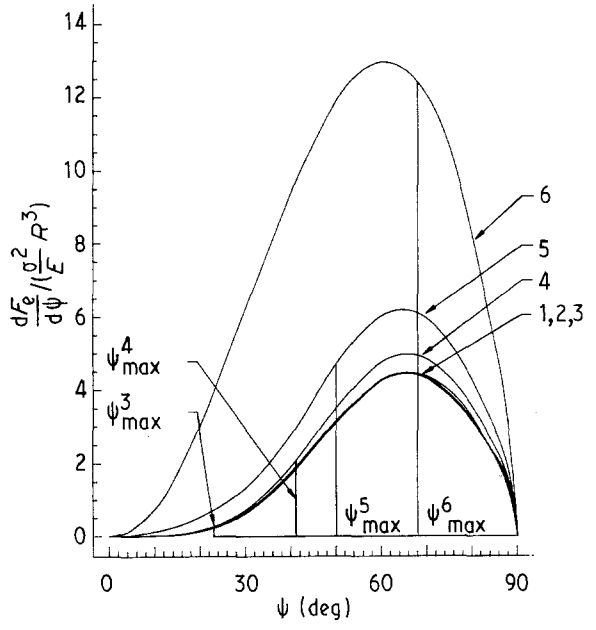

Figure 9 Dependence of spherical shell elastic energy, $dF_e(\psi)/d\psi$, on debonding angle, ψ, at different loads, σ = (1) 4 kg mm^{-2}, (2) 5.5 kg mm^{-2}, (3) 7 kg mm^{-2}, (4) 10 kg mm^{-2}, (5) 15 kg mm^{-2}, (6) $\sigma \gg \sigma_c$. The maximum debonding angles, $\psi^i_{max} = \psi_{max}(\sigma)$ in the presence of friction are marked by the vertical lines (i is the number of the corresponding curve): $\psi^1_{max} = 0°$, $\psi^2_{max} = 0°$, $\psi^3_{max} = 23°$, $\psi^4_{max} = 41°$, $\psi^5_{max} = 50°$, $\psi^6_{max} = 68°$.

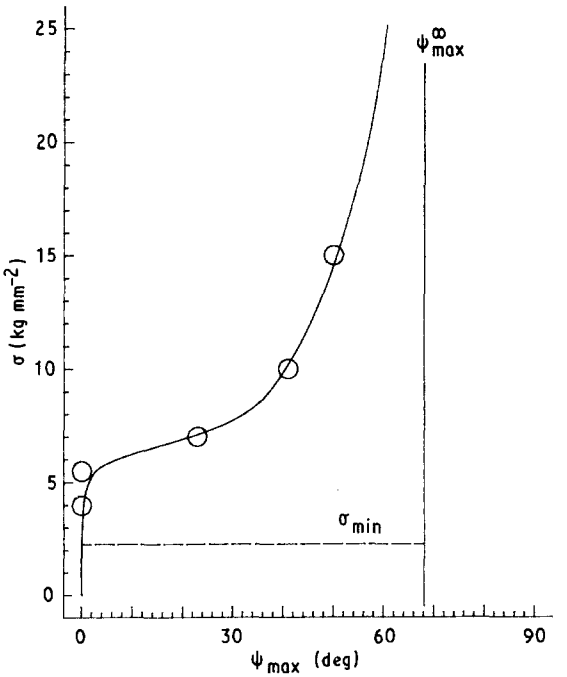

Figure 10 Dependence of maximum debonding angle, ψ_{max}, on applied stress, σ, in the presence of contraction and friction. (——) Maximum debonding angle reached at $\sigma \gg \sigma_c$, (– – –) minimum stress ($\sigma_{min} = \sigma_c/q_0$) required to detach the matrix from an inclusion in the presence of contraction.

made assuming a polydisperse structure model in the case of ideal bonding. The elastic modulus ratio of filler, matrix and coating was equal to 100:1:0.1. As is seen from Table I, composite stiffness changes slightly with coating thickness, h, in the considered diapason of h/R. At the same time, a rather strong h/R dependence of normal stress, σ_{11}, over the inclusion pole is observed. However, if $(h/R) < 10^{-3}$, soft coatings do not produce significant perturbations into the SSD in comparison with uncoated samples. From another point of view, the proper choice of thin coating makes it possible to modify the surface energy, γ, and friction at the interface.

3. Results and discussion

3.1. Materials and sample preparation

The matrix materials used were high-density polyethylene (HDPE, $MM = 12 \times 10^4$), isotactic polypropylene (PP, $MM = 15 \times 10^4$), and highly cross-linked epoxy polymer, resulting from polyaddition reaction of resorcinol diglycidyl ether and *m*-phenylenediamine under stoichiometric ratio of components [19]. A resorcinol diglycidyl ether was distilled over an argon flow in vacuum, and the aromatic amine was purified by vacuum quasisublimation at melting temperature $T_m = 64\,°C$. Glass spheres were used as a model filler. The glass particles were obtained in a variety of different size ranges and therefore they were sieved into sharp fractions of different average diameters (see Table IV below). The relief of the surface was about 0.1 μm (Fig. 13). The volume content of particles for all compositions was 0.5% to exclude agglomeration and particle interaction. The average distance between the inclusions corresponded to four diameters.

TABLE I Stress values, σ_{11}, at different points of the particle pole, and the effective Young's modulus, E_{ef}, for various thickness, h, of soft coating (C-coating volume content). Filler content is 3.7 vol %, correlation between filler, matrix and elastic modulus of the coating is 100:1:0.1, respectively

h/R	C(%)	E_{ef}	σ_{11}[a]			
			1.2	1.5	1.8	2.1
0.4	6.45	0.888	0.708	0.537	0.535	0.633
0.1	1.22	0.994	1.24	1.06	1.02	1.00
0.2	0.226	1.05	1.78	1.49	1.32	1.21
0.002	0.0222	1.08	1.97	1.67	1.45	1.31
0.0002	0.0022	1.08	1.99	1.69	1.46	1.32

[a] Relative distance (L/R) from particle centre.

Composite materials of glass sphere-filled HDPE and PP were prepared by melt mixing (HDPE on a two-roll mill at 170 °C for 15 min; PP in a Brabender mixer at 190 °C for 10 min) and compression moulding into thin plates under standard conditions. Dog-bone shaped samples were cut in accordance with ASTM D1708-66 and annealed (HDPE for 2 h at $T = 80\,°C$; PP for 1.5 h at $T = 90\,°C$).

In some experiments the modification of the interfacial boundary in composite materials based on PP was made by incorporation of 1% of a surface-active compound, octomethylcyclotetrosiloxane.

A special method was developed for epoxy resin composite preparation which excluded the appearance of air bubbles and provided a homogeneous distribution of glass spheres in the composite materials. The liquid compositions were initially degassed under continuous rotation at pressure $P = 1 \times 10^{-2}$ torr (1 torr = 133.322 Pa) and $T = 64\,°C$ for 10 min. Then the mixture was polymerized and rotated for 75 min at the same temperature in an argon atmosphere at normal pressure. It was then poured into a mould, consisting of two square glass plates held together with special rotating holder (rotation velocity $\Omega = 10\,min^{-1}$) and covered with dimethyldichlorosilane release agent. A two-step temperature regime ($T = 64\,°C$, 4 h; $T = 130\,°C$, 8 h) was used for final hardening. Tensile specimens were cut from the films and then annealed for 3 h at $T = 130\,°C$. The reaction yield and glass transition temperature were determined using a DuPont DSC. Ultimate reaction yield and glass transition temperature, $T_g = 135\,°C$, was achieved. Examination of the filled resin samples by optical microscopy showed a good distribution of particles and the absence of aggregation or settlement. The glass beads were coated with specially ultrathin polymer layers (polybutylacrylate, polystyrene, polydimethyl dichlorosilane) ~ 0.3 μm thick, to reduce the adhesive strength. The structure of the coating surface was studied with a Jeol-35C scanning electron microscope (SEM). The coating method will be discussed in a separate publication.

3.2. Equipment and testing methods

Apparatus for microdeformation and fracture study was devised consisting of an optical microscope with a video tape recorder and a special tensile testing machine, installed on its mechanical stage [20]. This apparatus allows specimens to be tested under

TABLE II Thermo-mechanical parameters, thermal contraction stresses, σ_c, and strains, ε_c, at the rigid particle surface for PE, PP and epoxy matrix

	ν_m	α_m ($\times 10^{-4}$)	$\varepsilon_c = \alpha_m \Delta T$ (%)	E_m^a (kg mm^{-2})	σ_c (kg mm^{-2})	σ_y^a (kg mm^{-2})
PP	0.34	3.2–4.0	3.2–4.0	74 ± 4	3.5–4.4	2.7 ± 0.07
PE	0.34	3.2–4.0	3.2–4.0	34 ± 3	1.6–2.0	1.7 ± 0.06
EP	0.33	~ 5.0	~ 5.0	240 ± 5	~ 1.8	9.2 ± 0.05

[a] Deformation velocity, $V_d = 2.5\,\%\,min^{-1}$.

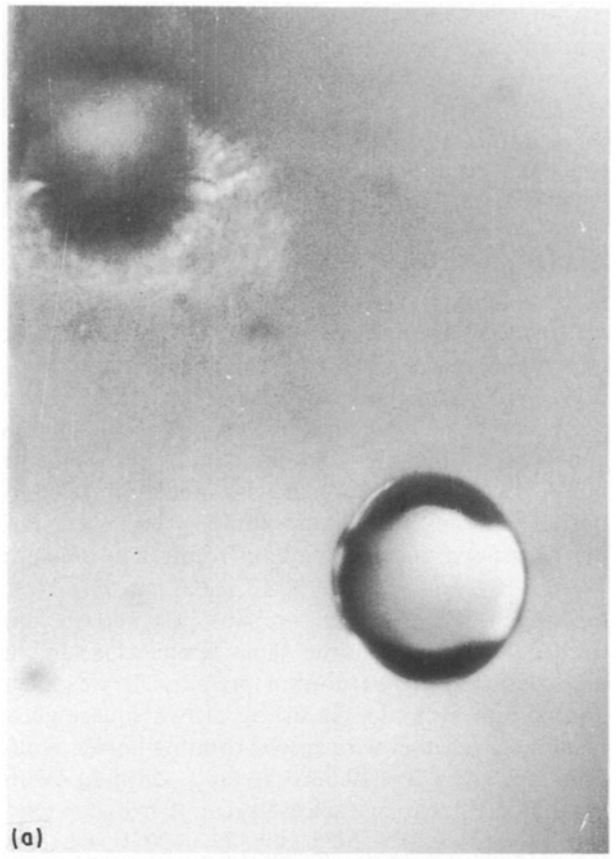

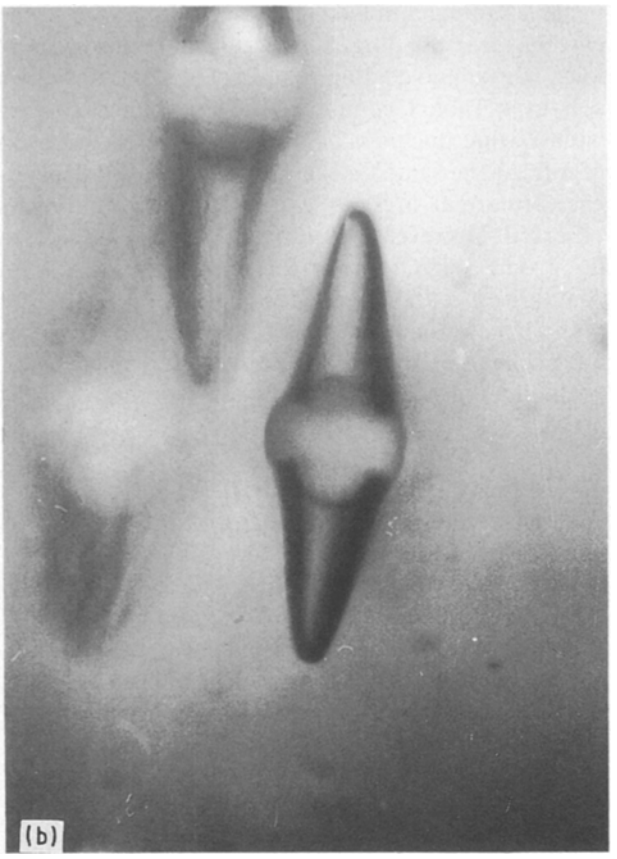

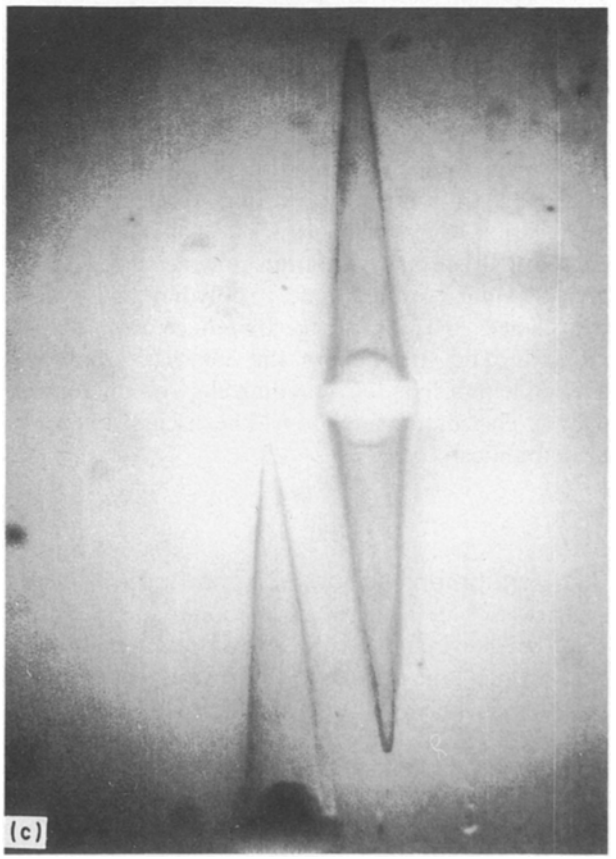

Figure 11 Light microscope micrograph of void initiation and growth in PE: (a) initiation of a debonding (appearance of the increasing darkening along the inclusion contour); (b) void formation during the debonding; (c) a void in the neck region.

different loading conditions directly in the microscope observation field. The tensile tests were performed at a strain rate $\dot{\varepsilon} = 2.5 \times 10^{-2}\ \text{min}^{-1}$. The measuring system is able to register stresses and strains in the course of time and at the moment of adhesive fracture.

Debonding was registered due to changes of stress-field configuration in the neighbourhood of the particles in the epoxy matrix (under transmitted polarized light, Fig. 11) and due to the appearance of darkening at the inclusion contours in PE and PP (dark-field image, Fig. 12).

3.3. Experimental analysis of debonding

The microscopic study of the polymer matrix debonding process from the spherical particles showed its critical character. An initial microcrack sited at the pole of an inclusion above a certain load propagates symmetrically up to a particular angle, ψ_d. The time of crack propagation was less then 0.5 s, which was much less than the loading time. Exfoliation at the other pole can occur as a result of the stress increase. The DA of the second crack is less than that of the first, because, the first crack appearance causes an alteration of the SSD.

This method of observation does not allow the initial of DA to be measured, but it can be confirmed that the angle is less than 10°.

The DSs are less than or near to 0.6 yield stress, σ_y, for all composite materials; this permits the use of elastic analysis as above [5, 15].

The debonding stresses and angles measured for an epoxy matrix and spherical differently covered

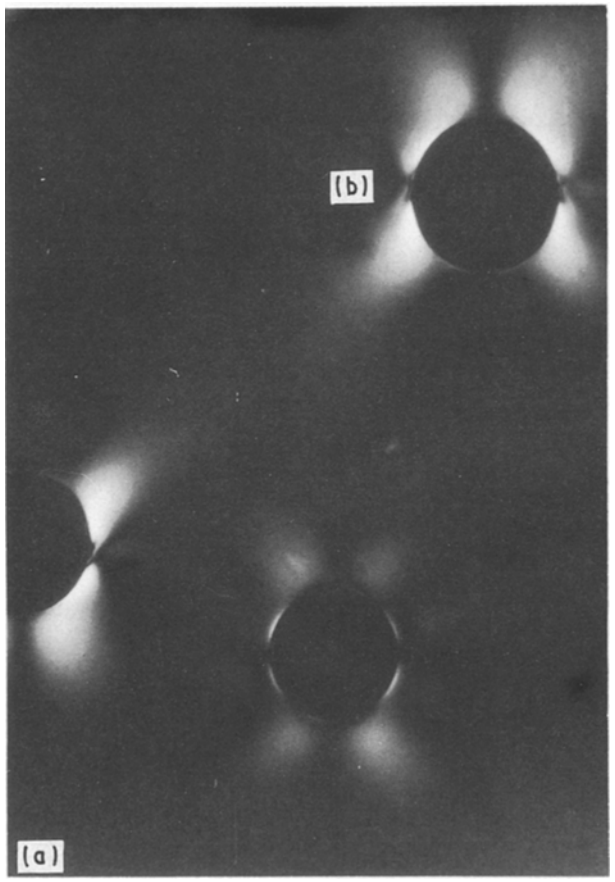

Figure 12 Polarized-light stress-field configurations for an epoxy matrix composition: (a) before debonding; (b) after debonding.

inclusions with a mean diameter 52 μm are given in Table III. The upper limits for local contraction stresses and strains calculated for this composition are given in Table II. It should be noted that chemical shrinkage and contraction stress relaxation was not taken into account in the calculations, but does occur in real systems. Comparison between debonding and contraction stresses for epoxy composite materials confirms the possibility of DA estimation without contraction.

Let us compare experimentally measured DAs with calculated ones without friction (Fig. 2). It is seen that final angles, ψ_2, can reach experimentally observed DAs (Compositions C, D, E, Table III) only at high $\bar{\gamma}$. An evaluated increase in $\bar{\gamma}$ would lead to high values of ψ_1, up to 45°. Such values might be measured experimentally. However, the angle size of the critical crack did not exceed 10°, as mentioned above. Experimentally obtained DAs are close to the value $\psi_{max} = 68°$, predicted assuming high friction.

The influence of different polymer coatings on the debonding stresses and angles can be analysed from the data shown in Table III. The thickness of the coatings was not greater than 0.5 μm or $\sim 10^{-3}$ from particle radius, and, according to the data presented in Table I, should not influence the local SSD of the composite. The DAs for the filler coatings based on polystyrene, polybutylacrylate and absorbed anchor polymer correspond to the values calculated for the high friction on the interfaces. On the other hand, for the polydimethyldichlorosilane coating, the decrease of DA is observed ($\psi_d \sim 60°$). SEM structure analysis of the coating surfaces indicates that minimal angles of debonding correspond to coatings with well-developed surface relief. The scanning electron micrographs of the polymer coatings on the glass beads are shown in Fig. 13. The influence of surface relief on the DA is similar to the influence of friction, and may be explained by the tangential mobility constraints of the polymer matrix layers adjacent to the filler surface. In the analysis carried out, the filler surface is supposed to be perfectly spherical, and in the case of exfoliation, the polymer matrix surface which has moved away from the particle is free and there is no restriction on any of its displacements, including tangential. Considering a well-developed filler surface, there is some possibility of tangential displacements restriction because of contact with bulges on the polymer coating, and subsequently some decrease of elastic energy release.

Calculations carried out of the crack opening dependence upon the angle and the surface structure analysis of the coatings allowed estimation of the decrease in DAs. For the Coatings A and B the mean height of inhomogeneities, d*h*, corresponds to 1 μm, and for Coatings B, G and D to 0.2 μm. From the relation between the height of the coating relief and debonding crack opening given in Fig. 8 it is possible to estimate the contact area and DA restriction. The angle of the debonding in that case will be $\psi_d = 60°$ corresponding to the experimentally obtained data.

During macrostress growth, a weak increase in DA is observed. For the composite with the butylacrylate copolymer filler coating, the increase in DA from 68° to 73° took place with increasing macrostress from $0.45\sigma_y$ to σ_y. The necessity of taking into account plastic deformations at these stresses hinders interpretation of the effect. In some cases, at high

TABLE III Debonding stress, σ_d, and angle, ψ_d, values for different thin polymeric coatings at a spherical particle (D = 52 μm) in an epoxy matrix: A, polydimethyldichlorosilane (particles were dried 30 min before in vacuum at T = 150 °C); B, polydimethyl-dichlorosilane (without previous degassing); C, polystyrene; D, polybutylacrylate; E, adsorbed layer of anchor polymer

	Epoxy				
	A	B	C	D	E
ψ_d(grad)	60(55[a])	61(58)	66(64)	68(61)	73(–)
σ_d (kg mm^{-2})	[b]	[b]	4.35 ± 0.03	4.27 ± 0.05	8.5 ± 0.2

[a] Mean angles of debonding formed at the opposite side of the particles are shown in parentheses.
[b] Stresses were too small to be measured by this method.

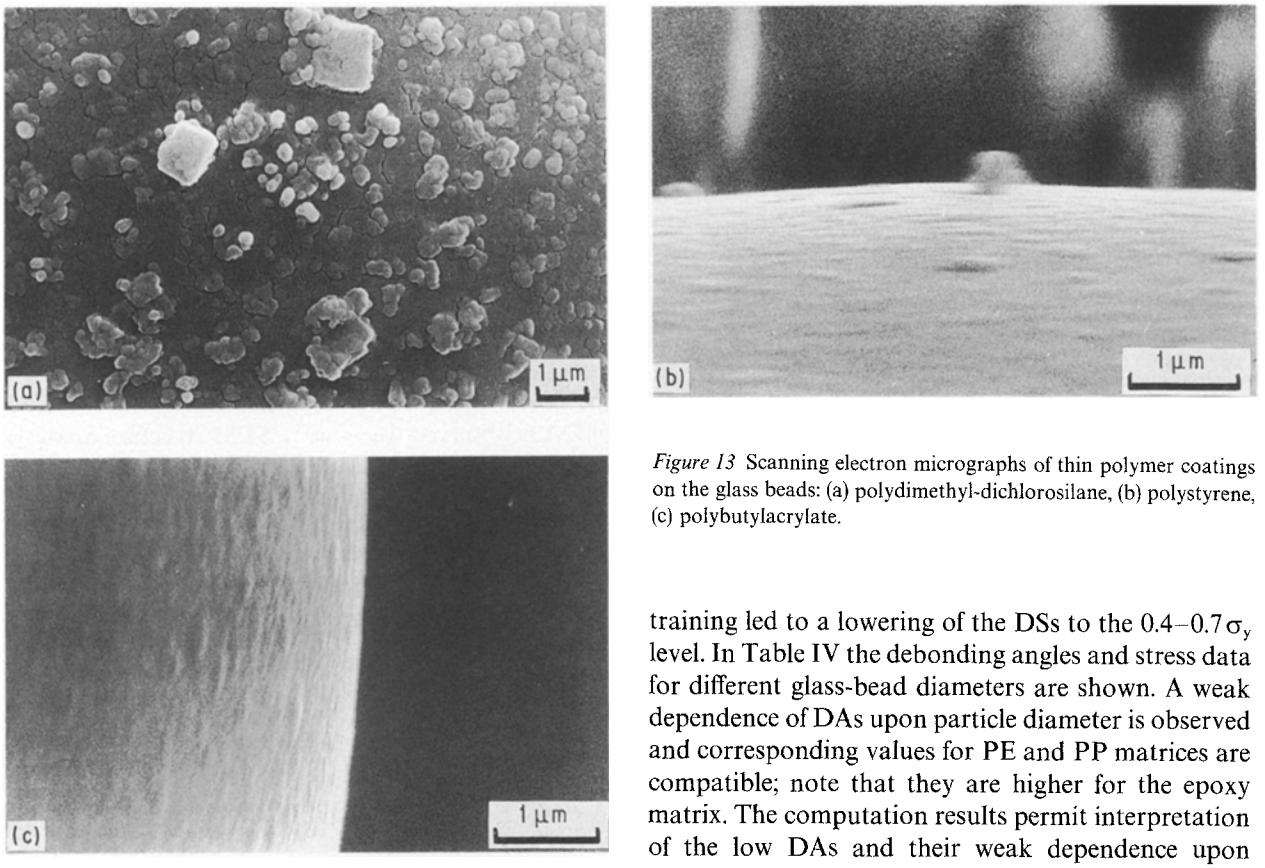

Figure 13 Scanning electron micrographs of thin polymer coatings on the glass beads: (a) polydimethyl-dichlorosilane, (b) polystyrene, (c) polybutylacrylate.

stresses debonding crack propagates into the matrix polymer before sample fracture [5].

According to Table III, DS depends upon the type of coating. The largest values of σ_d were observed for the adsorbed anchor polymer coating, and the minimum values for the dimethyldichlorosilane coating. The quantitative interpretation of this dependence is outside the scope of this article because of lack of γ values and initial defect sizes for the different coatings.

For PE- and PP-based compositions tested immediately after high temperature annealing, debonding was observed near or after the yielding limit of a material, apparently caused by high thermal contraction stresses (Table II). Therefore, in order to relax the thermal stresses before testing, the samples were kept at room temperature for 15 days. Such sample training led to a lowering of the DSs to the $0.4–0.7\sigma_y$ level. In Table IV the debonding angles and stress data for different glass-bead diameters are shown. A weak dependence of DAs upon particle diameter is observed and corresponding values for PE and PP matrices are compatible; note that they are higher for the epoxy matrix. The computation results permit interpretation of the low DAs and their weak dependence upon particle size as a consequence of friction and thermal contraction stresses commensurable with the DS. The diminution of a DA may also be caused by an increase in γ during debonding crack evolution, due to microplastic yielding in a crack-tip region. DA increases and exfoliation transforms into a microvoid when the applied stress increases (Fig. 12).

Analysis of the DS values for epoxy matrix and differently coated glass beads (Table III), PE and PP compositions, shows the dependence of σ_d both upon the polymer matrix and the modification of the interface boundary. The interface modification can be carried out either by treatment of the filler surface or incorporation of a surface-active compound (SAC) into the matrix volume. Data obtained for PP show that incorporation of the 1% organosiloxane does not affect polymer matrix mechanics, but reduces the DSs to 0.68 $kg\,mm^{-2}$ for the mean particle diameter $D = 52$ μm. This proves the interface state has a considerable influence on the DS in PP compositions. It

TABLE IV Debonding stress, σ_d, and angles, ψ_d, for different mean diameters, $\bar{D}$, of particles in PP and PE

$\bar{D}$	PP		PE	
(μm)	σ_d ($kg\,mm^{-2}$)	ψ_d (grad)	σ_d($kg\,mm^{-2}$)	ψ_d (grad)
8 ± 5	1.83 ± 0.17 1.67 ± 0.52[b]	55(51[a])	1.35 ± 0.1	58.6(54.6)
45 ± 3			1.09 ± 0.12	
52 ± 4	1.55 ± 0.19 0.68 ± 0.47[b]	58(57)	1.02 ± 0.1	57.3(54.5)
113 ± 9	1.16 ± 0.25			56.1(53.2)
180 ± 15	1.07 ± 0.25	57(55)		56.1(53.1)
360 ± 30	1.08 ± 0.19		0.73 ± 0.25	

[a] Mean angles of debonding formed at the opposite side of the particles are shown in parentheses.
[b] Debonding stress values for PP modified with surface-active compound.

should be noted that a scatter increase of the DSs after incorporation of organosiloxane SAC, points to its inhomogeneous distribution on the filler surfaces. The data discussed demonstrate the possible ways of DS regulation over wide limits.

According to the data shown in Table IV, an increase in particle diameter leads to diminishing DSs. As was noted in Section 2, the model under consideration allows the influence of particle diameter on the DS to be evaluated. Analysis of the data obtained shows that the dependence $\sigma_d(R)$ is weaker than the inverse square root dependence (Fig. 14) but stronger than the dependence presented in Fig. 5. It is supposed that defects of different sizes were initially distributed on the filler surfaces or were formed during loading. The uncertainty of the initial defect size makes it impossible to evaluate surface fracture energy, γ. In the absence of friction between crack faces, DA $\psi_d = \psi_2$ can be used for estimation of γ. In the opposite case of high friction, ψ_d weakly depends on $\bar{\gamma}$, so γ cannot be estimated from these data. The analysis carried out indicates the latter situation to exist.

In a general case, γ is an effective value and is determined not only by surface energy ($\gamma = \gamma_{mf} - (\gamma_m + \gamma_f)$, where γ_m, γ_f are the surface energy of matrix and inclusion, and γ_{mf} the interaction energy of matrix and inclusion), but also by the work of microplastic yielding during the process of debonding crack growth. In the given analysis, the contribution of microplastic yielding is not clear, but bearing in mind the low values of σ_d and the rigidity of the particle, it can be assumed to be insignificant.

Using the range of γ values (0.05–0.1 Jm^{-2}) given by Kinloch [21] for the polymer interface boundary fracture, it is possible to evaluate the range of critical defect radii, d, on the surface of the glass beads. In the case of an epoxy matrix and particle diameter $D = 50\,\mu m$, $\bar{\gamma} = 10^{-3}$–10^{-4}. For such $\bar{\gamma}$ values, ψ_1 is rather small ($d \ll R$) as shown in Fig. 4. So Equation 18 is valid and gives $d_{EP} = 0.015\,\mu m$. For PE, a similar evaluation gives $d_{PE} = 0.062\,\mu m$.

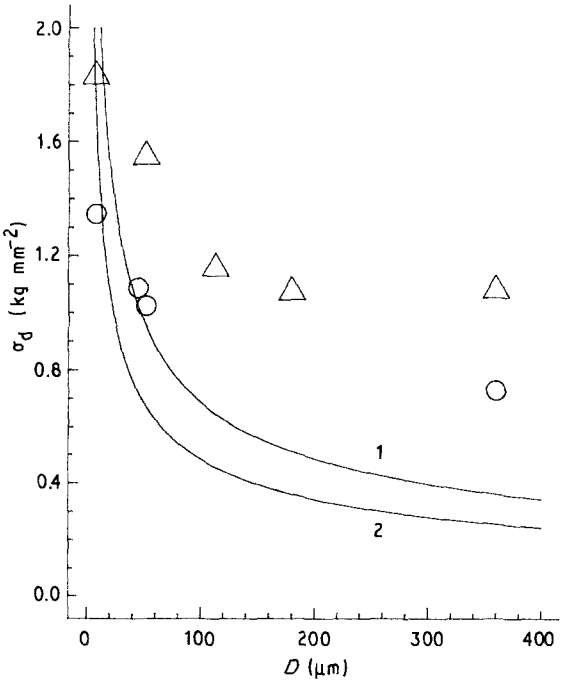

Figure 14 Experimentally observed dependence of debonding stress, σ_d, upon inclusion mean diameter for (△) PP and (○) PE matrix. (——) Approximations $\sigma = \text{const}\,R^{-0.5}$, obtained by the simple regression analysis ((1) PP, (2) PE).

Using the same range for γ and neglecting the contraction effect, it is also possible to estimate the minimum critical inclusion diameter, D_{cr}, at which debondings cannot appear. This critical value can occur in elastic approximation if there is some restricting stress, for example, yield point, σ_y. For the materials studied, $D_{cr}^{PE} = 0.1$–$0.2\,\mu m$, $D_{cr}^{PP} = 0.08$–$0.16\,\mu m$, $D_{cr}^{EP} = 0.02$–$0.04\,\mu m$. The corresponding values of D_{cr} are the bottom limits because the real values of γ can be greater. It should be noted that for inclusions with $D < D_{cr}$, a change of debonding mechanism can take place. The increase in load leads to the development of a plastic zone and debonding can occur due to the high interfacial displacement incompatibility at the particle surface. This seems possible, but requires special theoretical and experimental studies.

The analysis carried out shows the fruitfulness of the energy approach for the description of the debonding process in particle-filled materials. At the same time, the quantity of stored critical elastic energy is a necessary, but not sufficient, condition for debonding, because the existence of a certain size defect is supposed. According to estimation, the critical defect size is rather small ($d \ll R$). Probably the mechanism of critical defect formation will determine the scale factor of debonding.

In general DS will be determined by not only the elastic behaviour of the polymer matrix, reduced surface energy and particle size distribution, but also preparation and testing conditions.

In future publications, the nucleation mechanism of defects, crack path deflection from the interface into the matrix, and also the influence of plasticity, will be discussed.

4. Conclusions

1. The necessary energy conditions of interfacial crack propagation based on SSD numerical analysis in rigid spherical particle-filled composites, were formulated.

2. The values of the experimentally measured debonding angles, which are close to 68° and weakly depend on inclusion radius, debonding stress, and surface energy, were successfully described by the proposed model taking friction into account.

3. A contraction stress increase leads to an increase in debonding stress and a decrease of the debonding angle. Friction suppresses the shear mechanism of crack propagation and debonding becomes possible only at high loads.

4. A polydisperse structure model averages mechanical interaction between inclusions and so predicts the slight dependence of adhesive failure parameters on filler volume content. This influence is expected to be noticeable in regular structure models.

5. The observed scale effect cannot be described by the $\sigma_d \sim R^{-0.5}$ dependence and it is clear that a study

of defect-size distribution and the formation mechanism is necessary.

References

1. J. A. MANSON and L. H. SPERLING, in "Polymer blends and composites", Russian edition, edited by Yu. K. Godovsky (Khimiya, Moscow, 1979) p. 309.
2. M. E. I. DEKKERS and D. J. HEIKENS, *J. Mater. Sci.* **20** (1985) 3865.
3. J. SPANOUDAKIS and R. J. YOUNG, *ibid.* **19** (1984) 473.
4. V. G. OSHMYAN, N. N. KNUNYANTS, YU. M. TOVMASYAN, V. A. TOPOLKARAEV and L. I. MANEVICH, *Mehanika Kompozit. Materialov* **3** (1984) 431.
5. A. V. ZHUK, A. Y. GORENBERG, V. A. TOPOLKARAEV and V. G. OSHMYAN, *ibid.* **5** (1987) 776.
6. B. H. KAPIHALOO and K. VISWANATHAN, *J. Mater. Sci.* **20** (1985) 4103.
7. J. SPANOUDAKIS and R. J. YOUNG, *ibid.* **19** (1984) 487.
8. V. A. TOPOLKARAEV, N. V. GORBUNOVA, I. L. DUBNIKOVA, T. V. PARAMZINA and F. S. DYACHKOVSKY, *Vysokomolek. Soed.* **32A** (1990) 2210.
9. V. G. OSHMYAN, in "Proceedings of the 3rd Japan–USSR Joint Symposium on Advanced Composite Materials", Moscow, October 1991, edited by Yu. M. Tovmasyan (Institute of Chemical Physics, Moscow, 1991) p. 181.
10. A. A. GRIFFITH, *Trans. Roy. Soc. Lond.* **A221** (1920) 163.
11. Z. HASHIN, *AIAA J.* **4** (1966) 1411.
12. A. N. GENT, *J. Mater. Sci.* **19** (1984) 1947.
13. V. I. MOSSAKOVSKY and M. T. RYBKA, *Prikladnaya Matematika i Mehanika* **28** (1964) 1061.
14. R. W. DAVIDGE and T. J. GREEN, *J. Mater. Sci.* **3** (1968) 629.
15. V. G. OSHMYAN, Doctoral Thesis, Institute of Chemical Physics Academy of Sciences USSR (1987).
16. N. N. KNUNYANTS, M. A. LYAPUNOV, L. I. MANEVICH, V. G. OSHMYAN and A. Y. SHAULOV, *Mehanika Kompozit. Materialov* **2** (1986) 231.
17. Y. SATO and J. FURUKAWA, *Rubber Chem. Technol.* **35** (1962) 857.
18. *Idem, ibid.* **36** (1963) 1081.
19. L. M. CHEPEL, M. I. KNUNYANTS, V. A. TOPOLKARAEV, A. N. ZELENETSKY, O. B. SOLOMATINA and E. V. PRUT, *Vysokomolek. Soed.* **26A** (1984) 362.
20. V. P. YASHYN, I. S. VAINILOVICH, A. V. ZHUK, S. S. SHEIKO and S. N. MAGONOV, *Pribory i Tehnika Eksperimenta* **4** (1989) 246.
21. A. J. KINLOCH, *J. Mater. Sci.* **15** (1980) 2141.

Received 3 March
and accepted 21 October 1992